NUMERICAL INVESTIGATION ON HEATING PROCESS OF Ti/STEEL COMPOSITE PLATE IN A WALKING-BEAM REHEATING FURNACE

by

Zhanrui WANG, Boyan AN, and Hui YU*

School of Mechanical Engineering, Yanshan University, Qinhuangdao, China

Original scientific paper
https://doi.org/10.2298/TSCI231108082W

A 2-D numerical model was established to calculate the temperature distribution of Ti/steel composite plates in a walking-beam reheating furnace by using the central difference method. The heat transfer characteristics of Ti/steel composite plates in a walking-beam reheating furnace were studied. The influence of heating time, heating temperature, and different interface contact conditions in different heating zones on the temperature distribution of Ti/steel composite plates was studied. The results indicate that the maximum error between the calculated temperature and the measured temperature is 5.4%, proving the correctness of the numerical model. When heating continues, the plate cross-section temperature difference first increases and then decreases, with the maximum value of the temperature difference appearing in the preheating zone. There is a temperature inflection point at the interface between titanium plate and steel plate. The larger the proportion of vacuum zone in interface contact, the lower the plate center temperature.

Key words: *Ti/steel composite plate, walking-beam reheating furnace, temperature distribution, numerical model, heat transfer process*

Introduction

The Ti/steel composite plate combines the excellent properties of titanium plate and steel plate and is widely used in fields such as marine engineering and oil extraction. Many scholars have successfully prepared Ti/steel composite plates with different properties through rolling and explosion processes [1-3]. Reheating furnace is the main energy-consuming equipment in the steel rolling production line [4, 5]. It plays a critical role in the production of high-quality plate products [6]. The Ti/steel composite plates are placed in the reheating furnace and directly in contact with the high temperature gas in the reheating furnace. Heat is absorbed directly from the high temperature flue gas and furnace wall through convection and radiation and then transferred from the plate surface to the plate interior via heat conduction [7]. The research for the thermal control of reheating furnaces and the temperature-rising mechanism of plates has drawn a lot of attention during the last few decades.

Various commercial software such as FLUENT and opensource software OpenFOAM, as well as other CFD tools have been utilized to study the heating mechanism of the plates in the reheating furnace [8]. In this way, a great number of complicated calculated models have

*Corresponding author, e-mail: yuhui@ysu.edu.cn

been investigated. Kim *et al*. [9] first demonstrated that the sophisticated convection and radiation process could be developed quantitatively by the FLUENT software. Then a similar three-dimension model was developed by Kim *et al*. [10] and Hsieh *et al*. [11]. Jaklic *et al*. [12] devised an online graphical user interface that takes into account the geometric structure of the heating furnace and the heat exchange between pipes. Morgado *et al*. [13] built a model to mimic the erratic heating of billet and discovered that turbulence is directly connected to heat conduction. To better control the temperatures in various parts of the slab, Chena *et al*. [14] developed a model of energy distribution that shows the correlation between slab thermal efficiency, charging temperature and residence duration. Based on the finite difference method, Tang *et al*. [15] established a 2-D heat transfer model for the slab reheating process with the boundary conditions provided by simulation results from a 3-D CFD model. According to the gas circulation, the heat transfer, the geometric relationship, and the synchronous temperature data, Liu *et al*. [16] developed a slab heating model. By modeling a natural-gas fired walking hearth type furnace in detail, Prieler *et al*. [17] calculated the billet's transient heating characteristics regarding gas-phase combustion, heat transport, and combustion process, and revealed that 93% of the billet's total heat flux originated from radiation. In addition to CFD, some self-developed models were also applied. The user-defined function (UDF) was used by Garcia *et al*. [18] to analyze the contribution of solid and gas radiation to plate heating and found that around 25% of the radiation was absorbed by the plates provided by flue gases. A UDF was also developed by Han and Chang [19], and the influence of plate residence time was presented in their study. The role of the furnace burner was studied by Danon *et al*. [20, 21]. They found that the heat transfer, pollutant emission, and thermal efficiency have been affected by the burner. In the studies of Steinbeck *et al*. [22] and Yang and Luo [23], the plate was simplified into a 1-D model along with the plate thickness, which analyzed the heat exchange in the furnace and heat conduction of the plate. Luo and Yang [24] introduced an adjoint problem approach to solving the 2-D PDE in the furnace. Harish and Dutta [25] developed a model based on the finite volume method (FVM), which is capable of predicting the radiative flux and the plate temperature distribution. In addition, a transient movement of the plates was converted into a steady-state simulation through the introduction of source terms, which improved the computing efficiency [26].

For the previous analysis, researchers mostly focus on two areas: the temperature field and flow field in the furnace and the heat transfer between the furnace gas and plate, as well as how the plate conducts heat internally. However, previous research has focused on single-layer metal plates, with little research on the heating process of two or more metal composite plates. Therefore, a 2-D numerical model was established to calculate the temperature distribution of Ti/steel composite plates in a walking-beam reheating furnace by using the central difference method. The temperature change regularity of a Ti/steel composite plate in the heating process was discussed. In addition, the influence of several different interface contact conditions on the temperature distribution of Ti/steel composite plates was studied.

Method

Physical model

Figure 1 shows the geometric model of the Ti/steel composite plate during heating process. The Ti/steel composite plate is a kind of laminated metal composite material composed of titanium plate and steel plate in a laminated way, as shown in fig. 1(a). To distribute plates symmetrically when rolling, the two composite plates are placed together and separated by a

spacer. Each composite plate is 0.2 m thick, with a titanium plate to steel plate thickness ratio of 1:3. The length of Ti/steel composite plate in the model is 1 m. Figure 1(b) shows the structure of the walking-beam reheating furnace. The Ti/steel composite plates enter the reheating furnace from the left side of the reheating furnace and stay in the non-firing zone for a while. Then it passes through the preheating zone, heating zone I, heating zone II, and the soaking zone. Finally, the Ti/steel composite plates reach the final temperature in the soaking zone and exit from the right side of the reheating furnace.

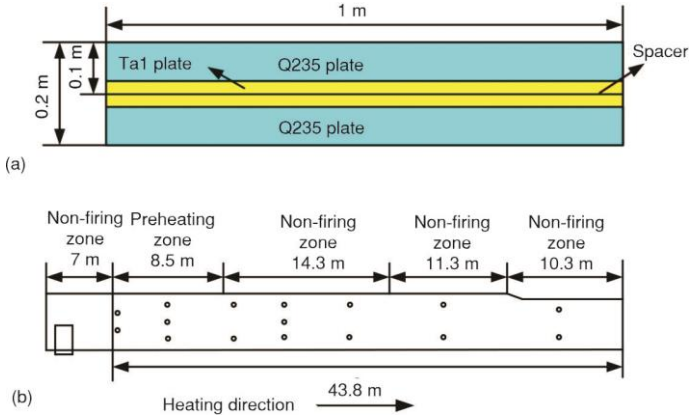

Figure 1. Geometric model; (a) structure of Ti/steel composite plate and (b) structure of walking-beam reheating furnace

Thermal conductivity and specific heat play a key role in the plate heating calculation, which significantly affects the temperature distribution of the plate. Differential scanning calorimetry and laser thermal conductivity meter were used to measure the specific heat capacity and thermal conductivity of metal materials, respectively. The thermal conductivity and specific heat of TA1 and Q235 were obtained through experiments, as shown in fig. 2. Plate temperature has little influence on the density, which is considered a constant: TA1: ρ = 4510 kg/m^3, Q235: ρ = 7850 kg/m^3 [27].

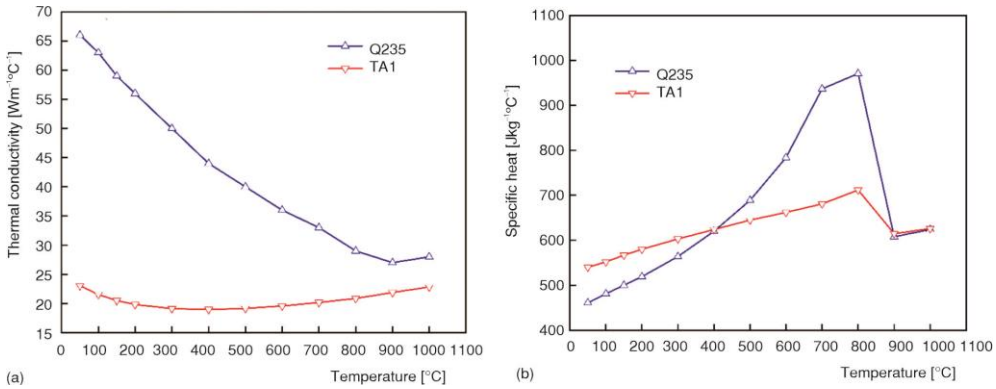

Figure 2. Material prosperity of the Q235 and TA1 with different temperature; (a) thermal conductivity and (b) specific heat

Numerical model

The governing equation describing the internal temperature distribution of the plate is the heat conduction equation. The general form of 2-D unsteady heat conduction differential equation in the rectangular coordinate system is [28]:

$$\rho c(T)\frac{\partial T}{\partial \tau}=\frac{\partial}{\partial x}\left[k(T)\frac{\partial T}{\partial x}\right]+\frac{\partial}{\partial y}\left[k(T)\frac{\partial T}{\partial y}\right]+S \tag{1}$$

where T, ρ, c, τ, and S are infinitesimal body temperature, density, specific heat, time, and per unit time per unit volume of the heat which is generated by the internal heat source, respectively. k is the thermal conductivity.

The analysis of heat exchange on the boundary is crucial to the overall calculation process, and it is crucial to consider convective heat transfer and radiative heat transfer in the heat flux on the boundary. The total heat transfer flux, q_0, can be expressed by [29]:

$$q_0=q_c+q_r=\alpha_c\left(T_f-T_m\right)+\alpha_r\left[\left(\frac{T_f}{100}\right)^4-\left(\frac{T_m}{100}\right)^4\right] \tag{2}$$

where q_c is the convective heat flux between the gas and plate surface, α_c – the convective heat transfer coefficient between the gas and plate surface, T_f and T_m are the gas temperature and plate surface temperature, q_r – the radiative heat flux on the plate surface, and α_r – the radiative heat transfer coefficient between the plate and furnace wall.

The FVM was employed to discretize PDE and a central difference method was developed when solving unsteady conduction problems. The heat transfer process is shown in fig. 3. The internal energy changes in the control body, P, from the time of t_0 to t_1 can be obtained according to the law of energy conservation:

$$U_P^1-U_P^0=Q_w^{0-1}+Q_e^{0-1}+Q_s^{0-1}+Q_n^{0-1}+S_P^{0-1} \tag{3}$$

where the superscripts (1,0 and 0-1) indicate time change, the left side of the equation $U_P^1-U_P^0$ is the energy increase of the control body, the right side $Q_w^{0-1}+Q_e^{0-1}+Q_S^{0-1}+Q_n^{0-1}$ is the heat energy that enters the control body from the four surfaces of the control body, S_p^{0-1} is heat source calorific value of the control body, namely the source term, and w, e, s, n, f, b represent the corresponding interface.

The discrete equation was constructed by the FVM. The obtained heat transfer equation is:

$$\begin{aligned}\left[\left(\overline{\rho(T)c(T)T}\right)_P^1-\left(\overline{\rho(T)c(T)T}\right)_P^0\right]\Delta x\Delta y=&\left[\left(\overline{k(T)\frac{\partial T}{\partial x}}\right)_e^{0-1}-\left(\overline{k(T)\frac{\partial T}{\partial x}}\right)_w^{0-1}\right]\Delta y\Delta t+\\&+\left[\left(\overline{k(T)\frac{\partial T}{\partial y}}\right)_n^{0-1}-\left(\overline{k(T)\frac{\partial T}{\partial y}}\right)_s^{0-1}\right]\Delta x\Delta t+\overline{S(T)}_P^{0-1}\Delta x\Delta y\Delta t\end{aligned} \tag{4}$$

To provide good model stability, the implicit scheme was introduced for discretization in this paper. The 2-D mesh used in a discretization process is shown in fig. 4. The discrete eq. (5) can be obtained using time implicit central differentiation schema on the eq. (4). By calculating the coefficients of the discrete equation, and then iteratively calculating, the heat transfer control equation is solved:

$$\left(\frac{\rho_P^1 c_p^1 \Delta x \Delta y}{\Delta t} - \frac{k_e^1 \Delta y}{\delta x_e} - \frac{k_w^1 \Delta y}{\delta x_w} - \frac{k_n^1 \Delta x}{\delta y_n} - \frac{k_s^1 \Delta x}{\delta y_s}\right) T_P^1 =$$
$$= \frac{k_e^1 \Delta y}{\delta x_e} T_E^1 + \frac{k_w^1 \Delta y}{\delta x_w} T_W^1 + \frac{k_n^1 \Delta y}{\delta y_n} T_N^1 + \frac{k_s^1 \Delta y}{\delta y_s} T_S^1 + \frac{\rho_P^0 c_P^0 \Delta x \Delta y}{\Delta t} + S_P^1 \Delta x \Delta y \quad (5)$$

where k_e, k_w, k_n, and k_s are the interfacial thermal conductivity between P and other control bodies, T_P, T_E, T_W, T_N, and T_S are the temperature of control body center point, respectively, and δx_e, δx_w, δy_n, δy_s are the distance between the control body center point P and adjacent control body center point.

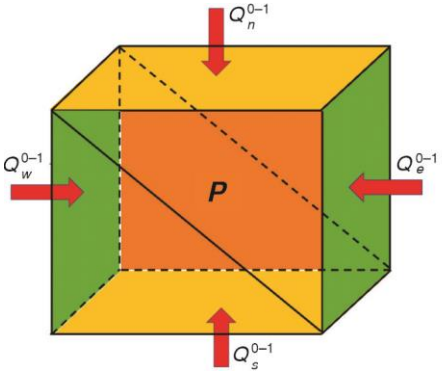

Figure 3. Heat transfer process

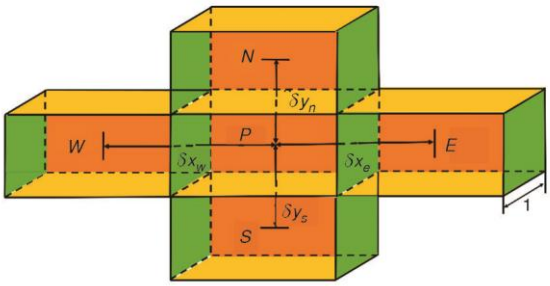

Figure 4. The 2-D mesh

Verification of numerical model

Based on field survey data, the initial temperature of the Ti/steel composite plate is set at 68 °C. The convective and radiative heat transfer coefficients are 15 W/m^2°C^4 and 0.8, respectively. The boundary conditions applied to the plate in the calculation are determined by the gas temperature in the reheating furnace. Figure 5 shows the temperature change curve of gas temperature in the reheating furnace measured on-site along the length of the reheating furnace. Each experimental measurement is performed three times, and the measurements are averaged. According to fig. 5, the temperature boundary conditions for preheating zone, heating zone I, heating zone II, and the soaking zone in the numerical model are 820 °C, 870 °C, 910 °C, and 925 °C, respectively. The heating times for preheating zone, heating zone I, heating zone II, and soaking zone are 50 minute, 70 minute, 70 minute, and 70 minute, respectively.

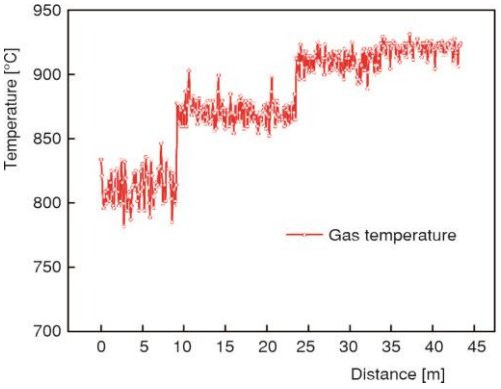

Figure 5. On-site furnace temperature

To measure the temperature of the Ti/steel composite plate in the reheating furnace, thermocouples are fixed on the surface and center of the plate, and a temperature recorder is connected to the thermocouple. Finally, the temperature changes on the surface and center of the plate

during the heating process were obtained, as shown in fig. 6. Figures 6(a) and 6(b) show the comparison between the calculated and measured temperatures of the surface and center of the Ti/steel composite plate, respectively. The calculated results are very consistent with the measured results. Figure 6(c) shows that the maximum error between the numerical and experimental results is 5.4%, indicating a good fit between the calculated and measured data, and the maximum error occurs in the preheating zone.

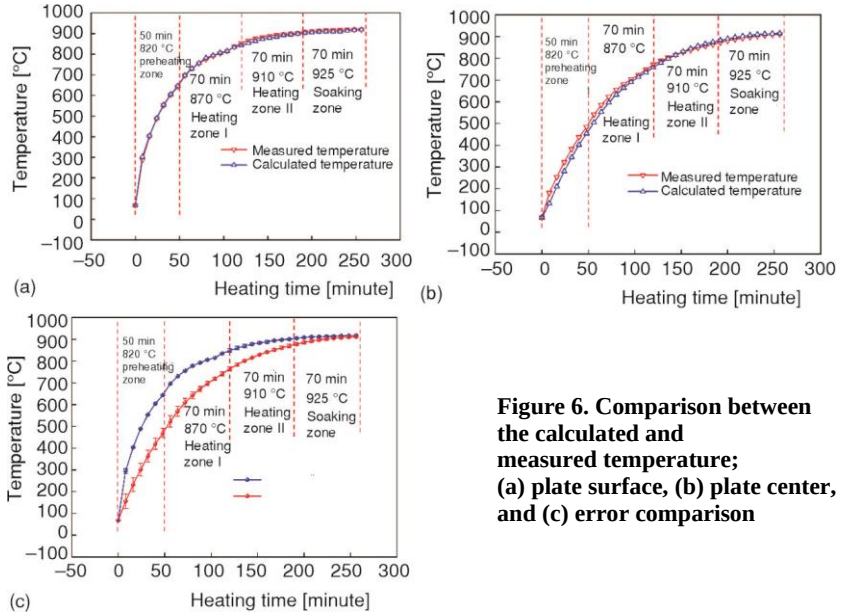

Figure 6. Comparison between the calculated and measured temperature; (a) plate surface, (b) plate center, and (c) error comparison

Results and discussion

Heat transfer characteristics of Ti/steel composite plates

Knowing the target temperature and the temperature difference inside the plate in the heating process is significant for the plate rolling. Figure 7 shows surface and center temperatures of the plate along with the heating time, as well as the cross-section temperature difference. Firstly, the overall temperature of the composite plate rises rapidly in the preheating zone and heating zone I on account of the large temperature difference between the plates and the furnace gas. The plate surface temperature rises to 650.35 °C rapidly in the preheating zone. As the plate enters heating zones I and II, the surface temperature of the plate increases up to 822.18 °C and 903.51 °C, respectively. The plate cross-section temperature difference first increases and then decreases, with the maximum value of the temperature difference appearing in the preheating zone, with a value of 208.29 °C. Similarly, the plate center temperature rises to 522 °C in the

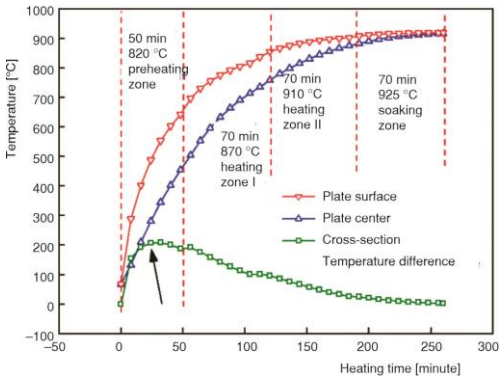

Figure 7. Plate temperature in the heating process

preheating zone. Then the plate center temperature reaches 724.77 °C and 878.85 °C when the plates leave heating zone I and heating zone II, successively. Until the heating time reaches 260 minute, the plates get to the plate outlet of the reheating furnace. At this time, the center temperature is 915.83 °C with a cross-section temperature difference of 3.25 °C.

Figure 8 shows the temperature distribution from the plate surface to the plate center at the different heating times (2 minute, 50 minute, 110 minute, and 190 minute). From the temperature distribution from the surface to the center of the plate, it can be seen that there is a temperature inflection point at 0.075 m, which is caused by the interface between the titanium plate and the steel plate. Titanium and steel have different material properties, with steel having a greater thermal conductivity than titanium. In addition, the slope of the temperature curve along the thickness direction gradually decreases. This indicates that the temperature difference from the surface to the center of the plate gradually decreases, and the temperature distribution at the plate center is more uniform than that on the plate surface. As the heating time goes on, due to the slow heat transfer from the surface to the center of the plate, the inflection point of temperature at the interface becomes more pronounced.

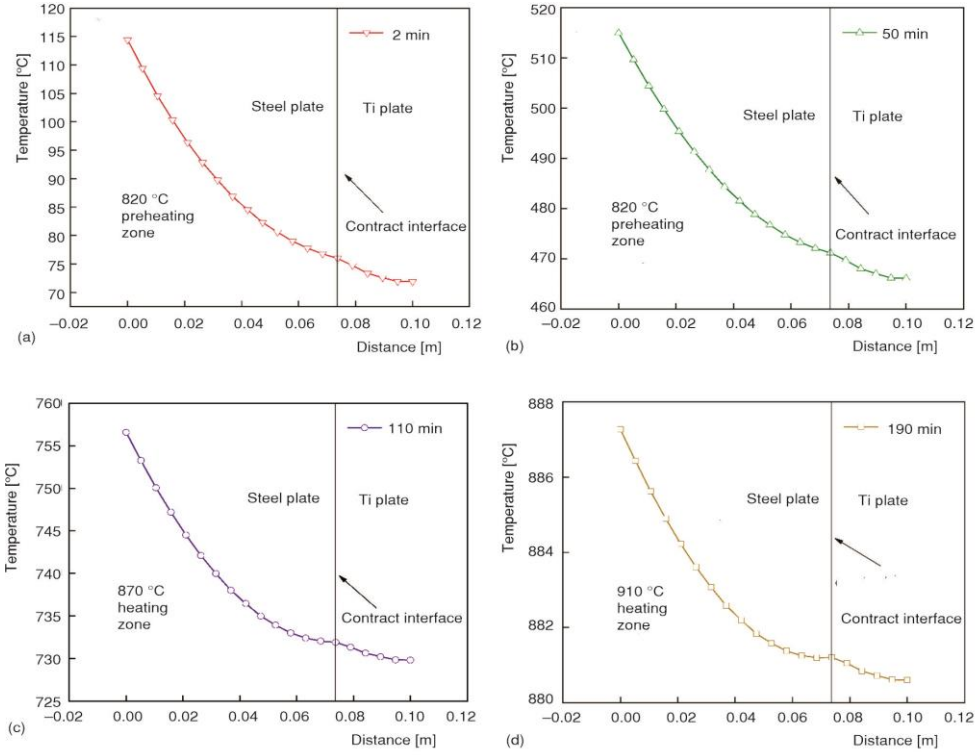

Figure 8. Temperature distribution from plate surface to center; (a) 2 minute, (b) 50 minute, (c) 110 minute, and (d) 190 minute

Influence of heating temperature and time on temperature distribution

Compared with the single plate, the temperature distribution of the Ti/steel composite plates before rolling has a higher requirement. In a walking-beam reheating furnace, the heating

time and temperature of each zone have a significant impact on the final temperature distribution of Ti/steel composite plates. Figure 9 shows the plate center temperature and plate cross-section temperature difference (the plate surface temperature minus the plate center temperature.) as the plate comes out of the reheating furnace at different heating temperatures in four heating zones. In fig. 9, when the heating temperature in each zone increases, the soaking zone has the greatest impact on the outlet temperature of the plate center, while the preheating zone has the smallest impact on the outlet temperature of the plate center. When the heating temperature of the soaking zone increases by 5 °C, the outlet temperature of the plate center increases by an average of 4.5 °C. When the heating temperature of heating zone I and heating zone II increases by 5 °C, the average change in the outlet temperature of the plate center is 0.15 °C and 0.66 °C, respectively. At the same time, the plate cross-section temperature difference at the outlet of the reheating furnace decreases with the increase of heating temperature in each heating zone, except for the soaking zone. When the heating temperature of the soaking zone increases by 5 °C, the plate cross-section temperature difference at the outlet of the reheating furnace increases by an average of 0.3 °C. When the heating temperature of heating zone I and heating zone II increases by 5 °C, the plate cross-section temperature difference decreases by an average of 0.1 °C and 0.5 °C, respectively. When the temperature of the preheating zone changes, there is no significant fluctuation in the cross-section temperature difference of the plate at the outlet of the reheating furnace.

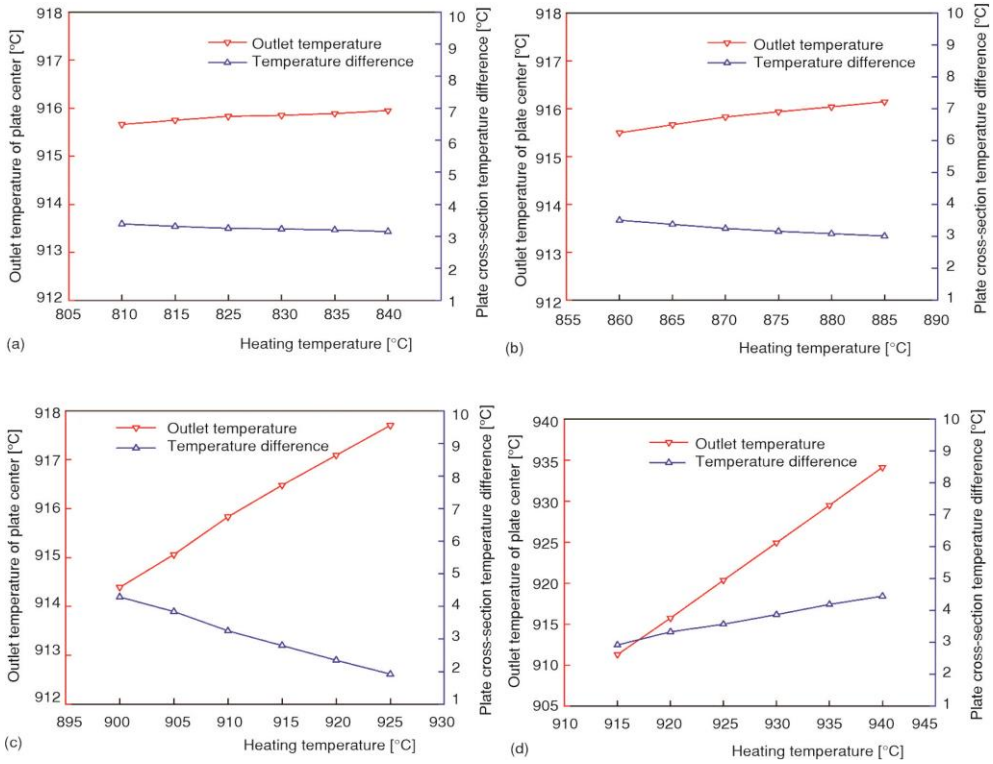

Figure 9. Outlet temperature of plate center and plate cross-section temperature difference with different heating temperatures; (a) preheating zone, (b) heating zone I, (c) heating zone II, and (d) soaking zone

Figure 10 shows the plate center temperature and plate cross-section temperature difference as the plate comes out of the reheating furnace at different heating time in four heating zones. As shown in fig. 10, the longer the composite plate stays in each heating zone of the reheating furnace, the higher the plate center temperature and the smaller the plate cross-section temperature difference will be when the plate leaves the reheating furnace. When the heating time in each zone increases, the soaking zone has the greatest impact on the outlet temperature of the plate center, while the preheating zone has the smallest impact on the outlet temperature of the plate center. When the heating time of the soaking zone increases by 5 minutes, the outlet temperature of the plate center increases by an average of 0.65 °C, and the plate cross-section temperature difference at the outlet of the reheating furnace decreases by an average of 0.5 °C. Similarly, when the heating time of the preheating zone, heating zone I, and heating zone II increases by 5 minutes, the outlet temperature of the plate center increases by an average of 0.28 °C, 0.36 °C, and 0.5 °C, respectively, and the plate cross-section temperature difference at the outlet of the reheating furnace decreases by an average of 0.23 °C, 0.29 °C, and 0.4 °C, separately.

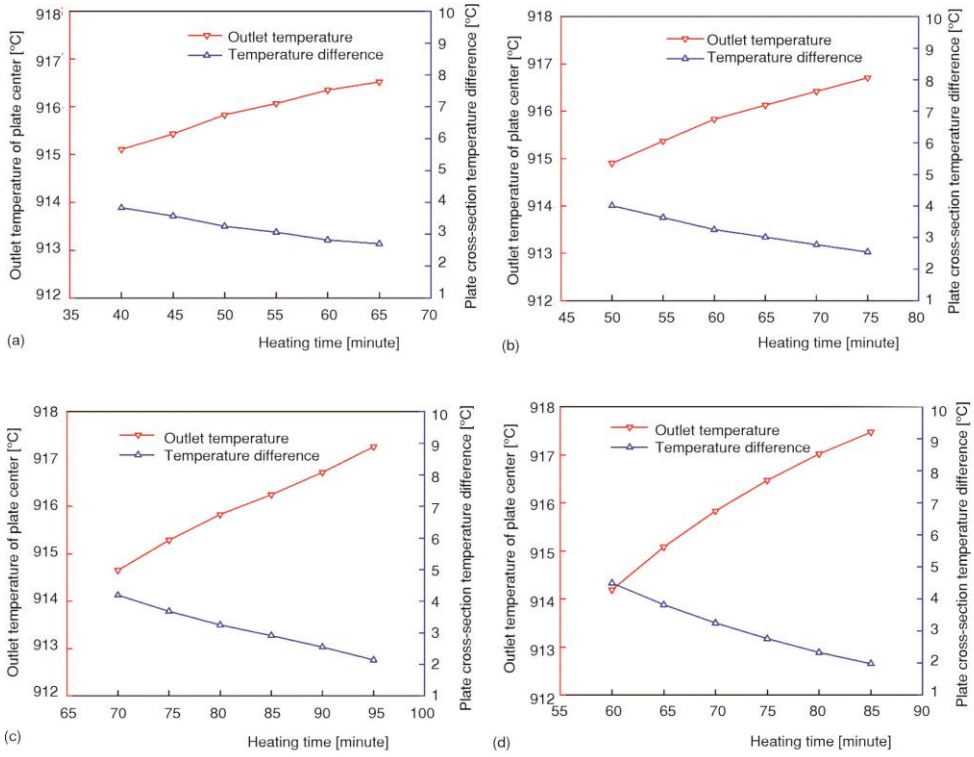

Figure 10. Outlet temperature of plate center and plate cross-section temperature difference with different heating time; (a) preheating zone, (b) heating zone I, (c) heating zone II, and (d) soaking zone

Influence of interface contact on temperature distribution

In the study of Ti/steel composite plate, the interface has always been the focus of attention. In the previous analysis, the temperature distribution under ideal contact conditions of different metals is mainly discussed. However, in most cases, the interface contact is not

idealized. Interface contact can be roughly divided into ideal contact, concave and convex face contact, and staggered contact. In the actual heating process, the roughness of the titanium plate and steel plate is generally up to the micron level, so the modeling will infinitely increase the amount of calculation. Therefore, four types of contact models are established to analyze the temperature distribution in the heating process of Ti/steel composite plates under different interface contact conditions from a macro scale, as shown in fig. 11. The four types of contact models are ideal contact, positive contact, staggered contact, and uneven contact. In uneven contact, three interface structures are established, with the base lengths of the triangle being 5 mm, 10 mm, and 15 mm, respectively. The non-contact region at the interface between titanium plate and steel plate is a vacuum region, and the form of heat transfer in the vacuum region is only thermal radiation transfer.

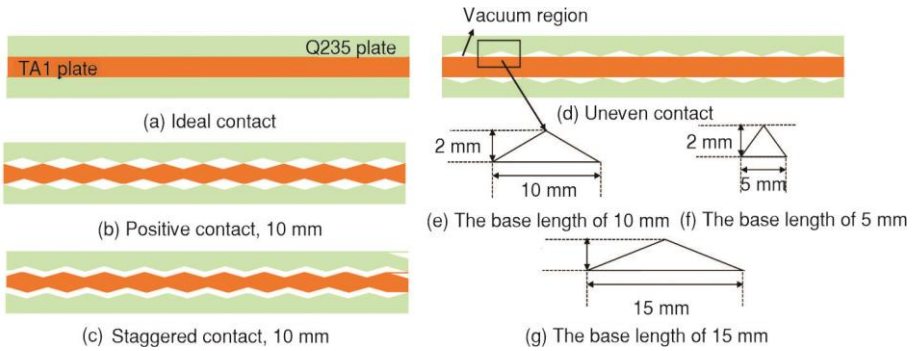

Figure 11. Different interface contact conditions

Figure 12 shows the temperature change of the plate center under different interface contact conditions. The overall trend of the temperature change of the plate center is similar. Figure 12(a) shows the temperature distribution at the plate center with different contact structures in uneven contact. In fig. 12(a), the larger the proportion of vacuum zone in interface contact, the lower the plate center temperature. That is to say, in uneven contact, the plate center temperature is the lowest when the interface structure is triangular with a base length of 15 mm. As the heating continues, the influence of the vacuum zone on the plate center temperature first increases and then decreases. When the heating time is 30 minute and 260 minute, respectively, the maximum temperature difference at the plate center in the four contact structures is 20.5 °C and 8.1 °C, respectively. Figure 12(b) shows the temperature distribution when the contact conditions are ideal contact, positive contact, staggered contact, and uneven contact. When the interface is in staggered contact, the temperature of the plate center is the lowest. When the interface is in positive and uneven contact, the temperature change at the plate center is relatively small compared to when the interface is in staggered contact. As the heating continues, the temperature difference between the staggered contact and the ideal contact first increases and then decreases. The maximum temperature difference with different contact styles occurs in heating zone I.

Figure 13 shows the temperature distribution of the plate under different interface contact conditions. After heating, the maximum temperature of the steel plate is distributed at the corner of the slab, with a maximum temperature of 920 °C. The temperature distribution of steel plates is generally similar. However, there is a large difference in the temperature distribution between the interface contact area and titanium plate, and there is an inflection point in the isothermal line at the interface contact area under all contact conditions, which is due to the

large difference of material properties and the emergence of vacuum region. Compared with ideal contact, the temperature inflection point of interface contact in non-ideal contact is more obvious, with the temperature inflection point in uneven contact being the most obvious.

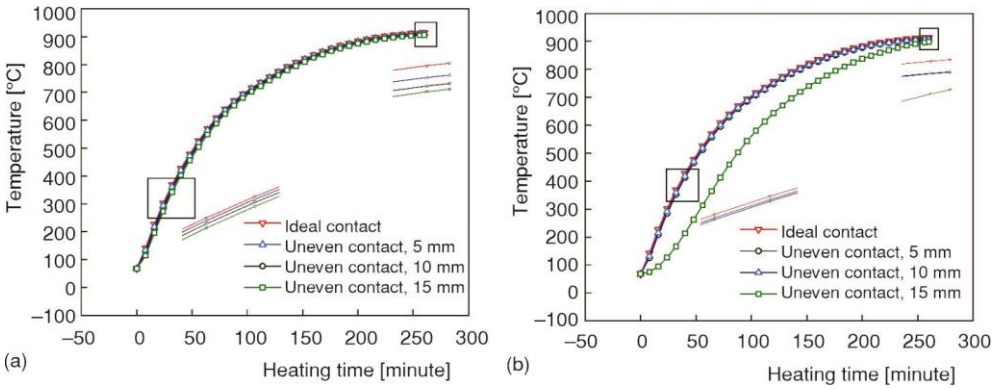

Figure 12. Temperature change of plate center under different interface contact conditions; (a) different contact structures in uneven contact and (b) different contact style

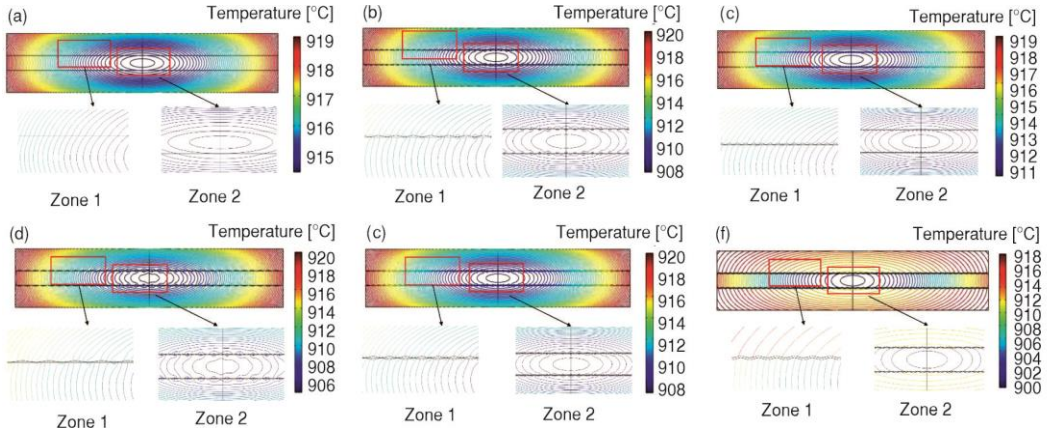

Figure 13. Temperature distribution of plate under different interface contact conditions; (a) ideal contact, (b) uneven contact, 10 mm, (c) uneven contact, 5 mm, (d) uneven contact, 15 mm, (e) positive contact, 10 mm, and (f) staggered contact, 10 mm

In figs. 12 and 13, it can be seen that no matter what kind of contact condition, the conduction at the temperature interface is related to the value of the contact area. With the increase in number and size of contact points, the heating process of composite plates becomes faster. Indicating that the larger the contact area, leads to the higher the heating efficiency of the composite plate. When there is no contact at the interface, the radiative heat transfer between the interfaces is main heat exchange mechanism, and the temperature transfer efficiency is low.

Conclusions

A 2-D numerical model to study the heating process of Ti/steel composite plates in a walking-beam reheating furnace was established in this study. The results of the numerical model were very consistent with the experimental results, with a maximum error of 5.4%. The main conclusions are as follows.

- The overall temperature of the composite plate rises rapidly in the preheating zone and heating zone I. The plate cross-section temperature difference first increases and then decreases, with the maximum value of the temperature difference appearing in the preheating zone. Due to the influence of different material properties and interface contact, there is a temperature inflection point at the interface between titanium plate and steel plate.
- When the heating temperature and time in each zone increases, the soaking zone has the greatest impact on the outlet temperature of the plate center, while the influence of the preheating zone is the smallest. Except for the soaking zone, the plate cross-section temperature difference at the outlet of the reheating furnace decreases with the increase of heating temperature in each heating zone.
- The larger the proportion of vacuum zone in interface contact, the lower the plate center temperature. As the heating continues, the influence of the vacuum zone on the plate center temperature first increases and then decreases. When the interface is in staggered contact, the temperature of the plate center is the lowest. When the interface is in positive and uneven contact, the temperature change at the plate center is relatively small compared to when the interface is in staggered contact. The maximum temperature difference with different contact styles occurs in heating zone I.

Acknowledgment

This work was supported by the Natural Science Foundation of Hebei Province (Grant No. E2021203237) and the Central Government Guides Local Science and Technology Development Fund Projects (Grant No. 216Z1002G).

Declaration of competing interest

The authors declare that they have no known competing financial interests or personal relationships that could have appeared to influence the work reported in this paper.

References

[1] Wu, Y., *et al*., Evolution Mechanism of Microstructure and Bond Strength Based on Interface Diffusion and IMCs of Ti/Steel Clad Plates Fabricated by Double-Layered Hot Rolling, *J. Mater. Process. Technol., 310* (2022), 117780
[2] Wu, Y., *et al*., Transverse Heterogeneity of Bonding Strength in Ti/Steel Clad Plates Fabricated by Hot Rolling with Bimetal Assembling, *Int. J. Adv. Manuf. Technol., 126* (2023), Apr., pp. 5033-5046
[3] Ren, Z. K., *et al*., Effect of Pulse Current Treatment on Interface Structure and Mechanical Behavior of TA1/304 Clad Plates, *Mater. Sci. Eng. A-Struct. Mater. Prop. Microstruct. Process., 850* (2022), 143583
[4] Han, Y., *et al*., Numerical Analysis of Flow Fields and Temperature Fields in a Regenerative Heating Furnace for Steel Pipes, *J. Therm. Sci. Eng. Appl., 10* (2018), 3, 031010
[5] Chakravarty, K., Kumar, S., Increase in Energy Efficiency of a Steel Billet Reheating Furnace by Heat Balance Study and Process Improvement, *Energy Rep., 6* (2020), Nov., pp. 343-349
[6] Tang, G. W., *et al*., CFD Modeling and Validation of a Dynamic Slab Heating Process in an Industrial Walking Beam Reheating Furnace, *Appl. Therm. Eng., 132* (2018), Mar., pp. 779-789
[7] Gu, M. Y., *et al*., Numerical Simulation of Slab Heating Process in a Regenerative Walking Beam Reheating Furnace, *Int. J. Heat Mass Transf., 76* (2014), Sept., pp. 405-410
[8] Ji, W. C., *et al*., Modeling and Determination of Total Heat Exchange Factor of Regenerative Reheating Furnace Based on Instrumented Slab Trials, *Case Stud. Therm. Eng., 24* (2021), 100838
[9] Kim, J. G., *et al*., Three-Dimensional Analysis of the Walking-Beam-Type Slab Reheating Furnace in Hot Strip Mills, *Numerical Heat Transfer: Part A: Applications, 38* (2000), 6, pp. 589-609
[10] Kim, M. Y., A Heat Transfer Model for the Analysis of Transient Heating of the Slab in a Direct-Fired Walking Beam Type Reheating Furnace, *Int. J. Heat Mass Transf., 50* (2007), 19-20, pp. 3740-3748
[11] Hsieh, C. T., *et al*., Numerical Modeling of a Walking-Beam-Type Slab Reheating Furnace, *Numer. Heat Tranf. A-Appl., 53* (2008), 9, pp. 966-981

[12] Jaklic, A., *et al*., Online Simulation Model of the Slab-Reheating Process in a Pusher-Type Furnace, *Appl. Therm. Eng., 27* (2007), 5-6, pp. 1105-1114
[13] Morgado, T., *et al*., Assessment of Uniform Temperature Assumption in Zoning on the Numerical Simulation of a Walking Beam Reheating Furnace, *Appl. Therm. Eng., 76* (2015), Feb., pp. 496-508
[14] Chen, D. M., *et al*., Bottleneck of Slab Thermal Efficiency in Reheating Furnace Based on Energy Apportionment Model, *Energy, 150* (2018), May, pp. 1058-1069
[15] Tang, G. W., *et al*., Modeling of the Slab Heating Process in a Walking Beam Reheating Furnace for Process Optimization, *Int. J. Heat Mass Transf., 113* (2017), Oct., pp. 1142-1151
[16] Liu, Y. W., *et al*., Performance of Fuel-Air Combustion in a Reheating Furnace at Different Flowrate and Inlet Conditions, *Energy, 206* (2020), 118206
[17] Prieler, R., *et al*., Prediction of the Heating Characteristic of Billets in a Walking Hearth Type Reheating Furnace Using CFD, *Int. J. Heat Mass Transf., 92* (2016), Jan., pp. 675-688
[18] Garcia, A. M., Amell, A. A., A Numerical Analysis of the Effect of Heat Recovery Burners on the Heat Transfer and Billet Heating Characteristics in a Walking-Beam Type Reheating Furnace, *Int. J. Heat Mass Transf., 127* (2018), Part B, pp. 1208-1222
[19] Han, S. H., Chang, D., Optimum Residence Time Analysis for a Walking Beam Type Reheating Furnace, *Int. J. Heat Mass Transf., 55* (2012), 15-16, pp. 4079-4087
[20] Danon, B., *et al*., Numerical Investigation of Burner Positioning Effects in a Multi-Burner Flameless Combustion Furnace, *Appl. Therm. Eng., 31* (2011), 17-18, pp. 3885-3896
[21] Danon, B., *et al*., Emission and Efficiency Comparison of Different Firing Modes in a Furnace with Four Hitac Burners, *Combust. Sci. Technol., 183* (2011), 7, pp. 686-703
[22] Steinboeck, A., *et al*., A Mathematical Model of a Slab Reheating Furnace with Radiative Heat Transfer and Non-Participating Gaseous Media, *Int. J. Heat Mass Transf., 53* (2010), 25-26, pp. 5933-5946
[23] Yang, Z., Luo, X. C., Optimal Set Values of Zone Modeling in the Simulation of a Walking Beam Type Reheating Furnace on the Steady-State Operating Regime, *Appl. Therm. Eng., 101* (2016), May, pp. 191-201
[24] Luo, X. C., Yang, Z., Dual Strategy for 2-Dimensional PDE Optimal Control Problem in the Reheating Furnace, *Optim. Control Appl. Methods, 39* (2018), 2, pp. 981-996
[25] Harish, J., Dutta, P., Heat Transfer Analysis of Pusher Type Reheat Furnace, *Ironmak. Steelmak., 32* (2005), 2, pp. 151-158
[26] Casal, J. M., *et al*., New Methodology for CFD Three-Dimensional Simulation of a Walking Beam Type Reheating Furnace in Steady State, *Appl. Therm. Eng., 86* (2015), July, pp. 69-80
[27] Zuo-Jiang, S., *et al*., A Thermal Field FEM of Titanium Alloy Coating on Low-Carbon Steel by Laser Cladding with Experimental Validation, *Surf. Coat. Technol., 452* (2023), 129113
[28] Jang, J. Y., Huang, J. B., Optimization of a Slab Heating Pattern for Minimum Energy Consumption in a Walking-Beam Type Reheating Furnace, *Appl. Therm. Eng., 85* (2015), June, pp. 313-321
[29] Dubey, S. K., Srinivasan, P., Development of Three Dimensional Transient Numerical Heat Conduction Model with Growth of Oxide Scale for Steel Billet Reheat Simulation, *Int. J. Therm. Sci., 84* (2014), Oct., pp. 214-227

Paper submitted: November 8, 2023
Paper revised: January 21, 2024
Paper accepted: February 22, 2024